Fragility of Surface States and Robustness of Topological Order in Bi_2Se_3 against Oxidation

Xiaoxiong Wang,[1,2,3] Guang Bian,[2,3] T. Miller,[2,3] and T.-C. Chiang[2,3]

[1]College of Science, Nanjing University of Science and Technology, Nanjing 210094, China
[2]Department of Physics, University of Illinois at Urbana-Champaign, 1110 West Green Street, Urbana, Illinois 61801-3080, USA
[3]Frederick Seitz Materials Research Laboratory, University of Illinois at Urbana-Champaign, 104 South Goodwin Avenue, Urbana, Illinois 61801-2902, USA

(Received 15 December 2011; published 29 February 2012)

Topological surface states are protected against local perturbations, but this protection does not extend to chemical reaction over the whole surface, as demonstrated by theoretical studies of the oxidation of Bi_2Se_3 and its effects on the surface spin polarization and current. While chemisorption of O_2 largely preserves the topological surface states, reaction with atomic O removes the original surface states and yields two new sets of surface states. One set forms a regular Dirac cone but is topologically trivial. The other set, while topologically relevant, forms an unusual rounded Dirac cone. The details are governed by the hybridization interaction at the interface.

DOI: 10.1103/PhysRevLett.108.096404 PACS numbers: 71.70.Ej, 73.20.At, 79.60.Dp

Surface states in topological insulators [1–4] are of great interest for spin information technology applications. These states are protected by time-reversal symmetry against local perturbations and are therefore quite tolerant to system imperfections and minor environmental effects [1,5–8]. This Letter addresses a key issue: can they be robust against oxidation, which can affect all air-exposed samples? Oxidation is also a processing step often employed in device fabrication, and its effects on the surface electronic and spin structure of topological materials are of great interest. It should be stressed that topological order, being a bulk property, is independent of the surface conditions, but the surface states and their spin properties can undergo drastic changes. We have chosen to perform a theoretical study of the oxidation of Bi_2Se_3. Among the known topological insulators [9–12], Bi_2Se_3 is one of the most technologically promising because of its wide band gap, a single Dirac cone, a simple structure, a natural cleavage plane, and its ease of preparation by molecular beam epitaxy [13]. However, its surface is prone to adsorption by residual gas [14], air [15], carbon monoxide [16], and oxygen [17], making it an excellent model system for the present study.

We perform first-principles calculations to determine the electronic structure of Bi_2Se_3 upon adsorption by molecular O_2 or atomic O, with an emphasis on the spin polarization and current that are relevant to applications. The nature of the chemical transformation is elucidated by following the parentage and heritage of the old and new surface states. While chemisorption of O_2 largely preserves the topological surface states, reaction with atomic O removes the original surface states and yields two new sets of surface states with unusual features. Although the topological constraint of the substrate guarantees that one (and only one) of the two sets must be topologically relevant, the surface spin current is very much reduced. This finding shows that air exposure can be a serious concern for such materials, and surface states of pristine topological insulators are not necessarily relevant to applications.

Our calculations were performed using a density functional approach within the local density approximation. The wave functions and eigenvalues are evaluated using the Abinit package [18,19], from which we compute the charge separation, spin polarization, spin current, and other quantities of interest. The computation was based on a plane-wave basis, with the cutoff energy set at 400 eV. Reciprocal space sampling was carried out with a $4 \times 4 \times 1$ grid. The Hartwigsen-Goedecker-Hutter pseudopotential used in the computation is fully relativistic, but the spin-orbit coupling can be manually turned off. We employed the experimental lattice constants for the lattice structure of Bi_2Se_3.

The structure of Bi_2Se_3 consists of a periodic stacking of quintuple layers (QLs) [9], with each QL made of three Se atomic layers intercalated by two Bi atomic layers [20]. The inter-QL bonding is weak, and the stable surface is an outer Se atomic plane of a QL. Calculations for various slab thicknesses were performed. The surface states of bare slabs thicker than about six QLs were essentially independent of the slab thickness, implying that the interaction or overlap of the surface states associated with the two faces of the slab could be ignored for the thicker slabs [21]. We employed a slab thickness of 10 QL in the final calculations in order to be well above this limit. A supercell geometry was employed, with the spacing between neighboring slabs set at 15 Å. The equilibrium adsorption geometries of O_2 and O on the surface were determined by minimizing the forces to less than 1×10^{-6} hartree/bohr.

Reaction of Bi_2Se_3 with oxygen gas initiates with the adsorption of molecular O_2. Calculations show that O_2 adsorbs on a surface Se atom in a linear straight-up configuration. The O-O bond is slightly elongated (1.37 vs

1.21 Å), suggesting a weakened molecular bond. The chemisorption bond, with a bond energy of 0.12 eV, is weak [22]. For reference, the band structure of a pristine 10-QL slab of Bi_2Se_3, presented in Fig. 1(a), shows two topological surface bands, $A_{1,2}$. The other bands are quantum-well states. The shading indicates the projected bulk band regions. Bands $A_{1,2}$ intersect at the Dirac point DP_A to form a Dirac cone. The band structure after O_2 adsorption [Fig. 1(b)] shows a similar Dirac point at $DP_A{}'$. The additional bands in the gap are derived from the $2p_{x,y}$ states of O_2. The $2p_z$ bonding states, at lower energies, are outside the display area of the figure. The chemical interaction, though weak, causes $A_{1,2}$ to hybridize with the $2p$ bands of O_2 [23], resulting in a small anticrossing gap.

Further oxidation results in the dissociation of O_2 [17] and the bonding of each surface Se atom by an O atom directly atop at a Se-O bond length of 1.72 Å. The calculated bond energy is 4.5 eV. With the bond energy of O_2 being 5.2 eV [24], oxidation of the surface is highly exothermic with an excess energy of $2 \times 4.5–5.2 = 4.2$ eV. The calculated band structure [Fig. 1(c)] reveals two surface state pairs $B_{1,2}$ and $C_{1,2}$, which cross at DP_B and DP_C, respectively. DP_B is Dirac-like, but both bands $B_{1,2}$ merge into the valence band region and are topologically trivial. By contrast, bands $C_{1,2}$ are parabolic near the zone center. The result is a highly unusual rounded (rather than pointed) Dirac cone with a finite effective mass. These bands span the bulk gap, and the topological order of the system is preserved. Calculations for the same oxidized slab but with the spin-orbit coupling turned off [Fig. 1(d)] show that the band gap is no longer spanned by surface states, and the system becomes topologically trivial.

The above results [Figs. 1(a) and 1(c)] do not reveal the connection between the original surface states and the new ones. We resolve this question by placing the oxygen atoms far away from the substrate, where the interaction with the substrate is minimal, and then moving the oxygen atoms gradually to the equilibrium bonding positions. With the O-Se bond stretched by 1.2 Å [Fig. 2(a)], the original surface state pair can be identified with a slightly altered crossing point at $DP_A{}'$. The other states in the gap are derived from the mostly decoupled oxygen $2p$ states. Reducing the O-Se stretch to 0.8 Å [Fig. 2(b)] pushes $DP_A{}'$ downward, and the oxygen states split and develop

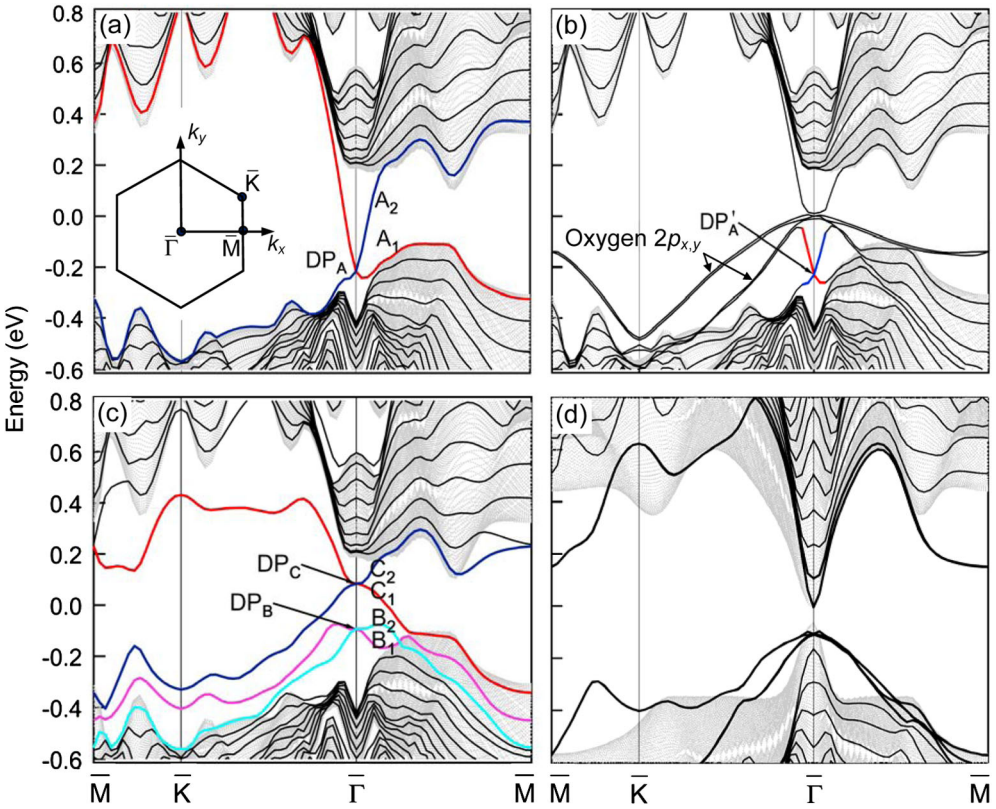

FIG. 1 (color online). Calculated band structures of pristine and O_2- and O-adsorbed Bi_2Se_3. (a) Results for a 10-QL slab of Bi_2Se_3. The shading indicates the projected bulk band regions. Bands $A_{1,2}$ are spin-polarized surface states; they cross at the Dirac point DP_A. (b) Results after surface adsorption of O_2. The Dirac point moves slightly to $DP_A{}'$. The other bands in the gap are derived from the oxygen $2p$ states. (c) Results after surface adsorption of atomic O. Bands $B_{1,2}$ and $C_{1,2}$ are surface states; they cross at DP_B and DP_C, respectively. Pair $C_{1,2}$ spans the band gap. (d) Results for O-adsorbed Bi_2Se_3 but with the spin-orbit coupling turned off in the calculation.

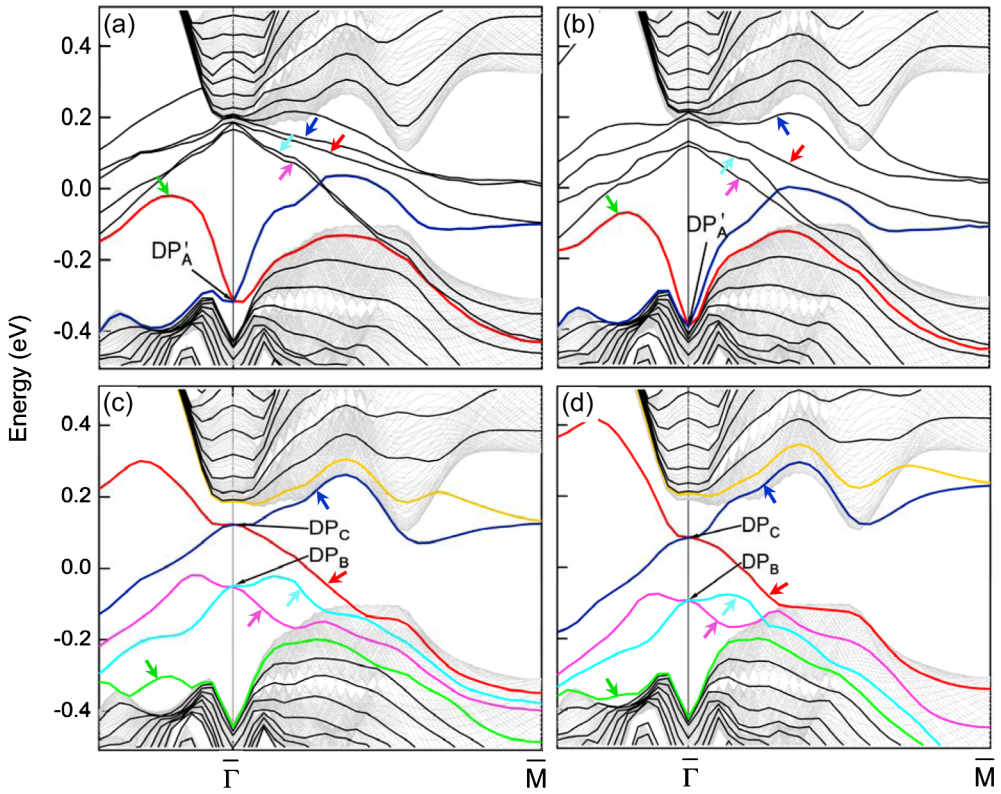

FIG. 2 (color online). Evolution of the surface states upon O adsorption on both faces of a 10-QL Bi_2Se_3 slab. The distance of the O to the Se surface atom is stretched from the equilibrium distance by (a) 1.2 Å, (b) 0.8 Å, (c) 0.3 Å, and (d) 0.0 Å. The arrows point to the bands that evolve with the changing distance.

more complex shapes. As the O atoms further approach the Se, the original surface states move into the valence band region [Fig. 2(c)]. Finally, the oxygen-derived states become the new surface states [Fig. 2(d)]. It is interesting to note that when $DP_A{}'$ merges into the valence band region, DP_C moves into the gap, and the topological order of the system is maintained throughout the process. This Dirac point tuning, however, cannot be (easily) realized experimentally.

The slabs, with or without adsorbed oxygen on both faces, have inversion symmetry. Consequently, all states form spin-degenerate Kramers doublets [25]. The two surface states in a doublet are separately localized near the two faces of the slab [26] in accordance with the Rashba interaction [27,28]. All bulk-derived doublets should exhibit no such charge and spin separations in the bulk limit, but small separations can occur in thin films. To quantify these properties, we define, for each band along the $\bar{\Gamma}\bar{M}$ (k_x) direction, a charge-separation function:

$$\Delta C(k_x) = \frac{2}{D}\sum_i \langle \Psi_i(k_x)| \, |z| \, |\Psi_i(k_x)\rangle - 1, \qquad (1)$$

where D is the slab thickness, $z = 0$ is at the midpoint of the slab, and the summation is over the two states in each Kramers doublet. This function ranges from $+1$ (charge concentrated at the surfaces at $z = \pm D/2$), to 0 (uniform distribution), and to -1 (charge concentrated at the midplane of the slab). Likewise, we define a spin-polarization (or spin-imbalance) function:

$$P(k_x) = \frac{1}{\hbar}\sum_i \langle \Psi_i(k_x)|s_y \mathrm{sgn}(z)|\Psi_i(k_x)\rangle, \qquad (2)$$

where sgn(z) is the sign function, and s_y is the spin operator along y, the only direction yielding a nonzero spin polarization by symmetry. This function equals ± 1 if the top (bottom) half of the slab carries an electron with its spin fully polarized along $\pm y(\mp y)$. The y-polarized spin current along the x direction is given by

$$I(k_x) = P(k_x)\frac{v_x(k_x)}{v_0} \qquad (3)$$

where v_x is the x component of the group velocity. I is normalized to ± 1 for a surface state doublet with a full spin imbalance and traveling at the characteristic velocity of $v_0 = \hbar k_{\bar{\Gamma}\bar{M}}/m$, where m is the free electron mass.

The values of ΔC, P, and I for a bare 10-QL slab of Bi_2Se_3 are computed for $A_{1,2}$ and the two neighboring quantum-well bands P and Q [Figs. 3(a)–3(d)]. Bands $A_{1,2}$ exhibit large ΔC, P, and I within the band gap. These properties diminish as the surface states disperse away from the zone center, approach, and eventually merge

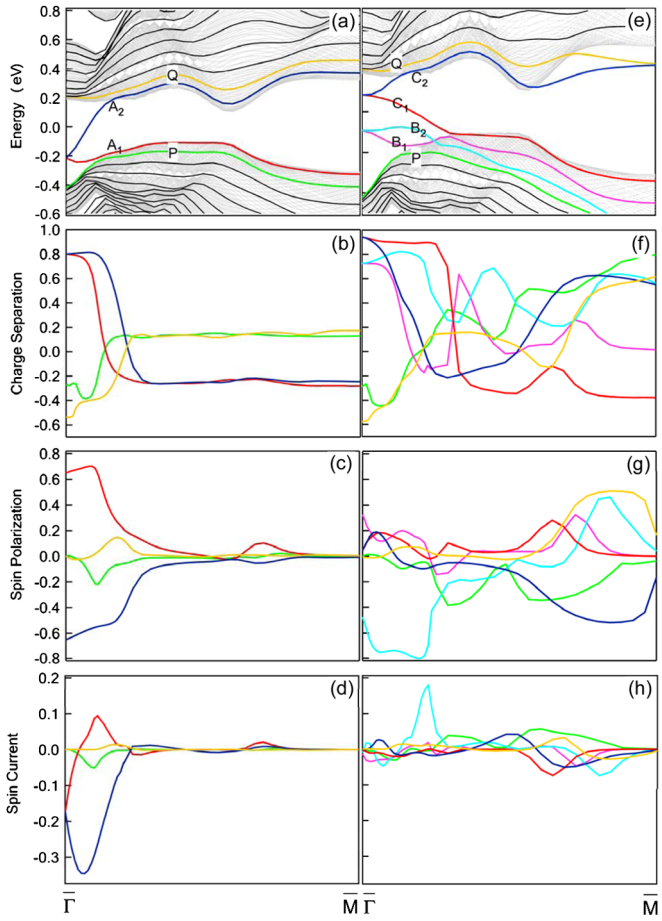

FIG. 3 (color online). Spin and charge properties of the bands in Bi_2Se_3 and Bi_2Se_3-O. (a) Band dispersion relations for a 10-QL slab. $A_{1,2}$ are surface bands, and P and Q are the two neighboring quantum-well bands. (b) Charge separation ΔC. (c) Spin-polarization P. (d) Spin current I. (e)–(h) Corresponding results for Bi_2Se_3-O. The curves are color coded.

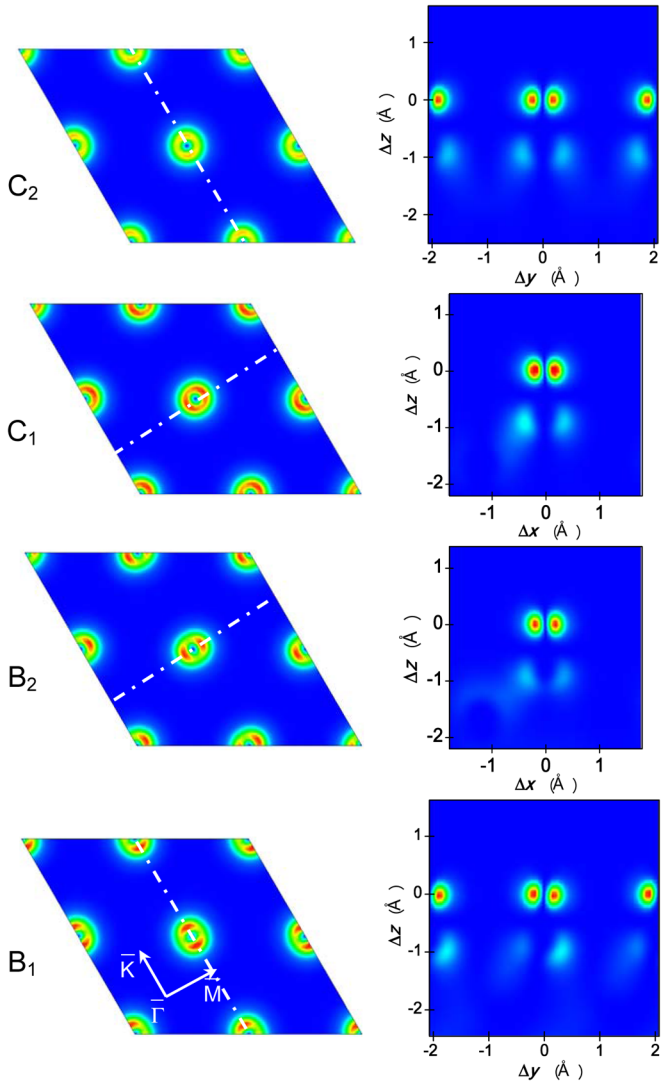

FIG. 4 (color online). Charge density distributions for the surface states in Bi_2Se_3-O. The left panels show the charge distributions within the oxygen plane in a 2×2 surface cell. The dash-dotted lines show where a vertical cut is made in each case; the results of the cuts are shown in the right panels. Δx, Δy, and Δz are distances referred to an adsorbed oxygen atom.

into the bulk region. Bands P and Q show little spin polarization near the zone center but have a negative charge separation, meaning that the charge density is suppressed near the slab faces. Because of the tendency toward charge neutrality within the slab, the accumulated surface charge from the surface states must be compensated for by a reduction of charge associated with nearby quantum-well states.

The above results are qualitatively as expected based on the Rashba interaction [27,28]. The corresponding results for Bi_2Se_3-O [Figs. 3(e)–3(h)]) are substantially more complex. States $B_{1,2}$ and $C_{1,2}$ all show a strong charge separation within the gap. However, their charge separations and those of the neighboring quantum-well bands P and Q show complex variations outside the gap (at larger k_x). The reason is a strong hybridization of these bands with the O states, resulting in a significant surface charge. The spin-polarization functions also show complex variations for a similar reason. The key quantity of interest to applications, the spin current, is generally much weaker after oxidation. The large reduction for $C_{1,2}$, which span the bulk gap and would be candidates for surface transport, is partly caused by the smaller group velocities of the bands within the gap. Because of the parabolic dispersions at the zone center, the spin current actually vanishes there.

The characters of $B_{1,2}$ and $C_{1,2}$ are clarified by the calculated charge distributions at a point close to the zone center ($k_x \rightarrow 0$). Figure 4 presents charge distributions within a 2×2 surface cell in the oxygen plane (left panels); the dash-dotted lines indicate where xz and yz cuts are made to reveal the vertical distributions (right panels). The charge, strongly concentrated around each O atom, shows the oxygen $2p_{y,x}$ orbital characters for $B_{1,2}$,

respectively. For $C_{1,2}$, the orbital characters are $2p_x \pm i2p_y$ with an azimuthally isotropic donut-shaped distribution. All of these oxygen-derived states hybridize with the substrate states, but $C_{1,2}$ involve mostly just the $4p$ states associated with the top Se atomic layer [20]. The topological states $C_{1,2}$ are thus well isolated from the underlying Bi_2Se_3 crystal structure that is the source of the global topological order; this nonlocal quantum interaction implies interesting engineering possibilities. The orbital angular momentum along y is effectively quenched for $C_{1,2}$, and the Rashba splitting vanishes to first order. The splitting away from the zone center is a second-order effect, which accounts for the parabolic dispersions of $C_{1,2}$. By contrast, states $B_{1,2}$ contain a significant mixture of Bi_2Se_3 states and have a finite Rashba splitting [20].

For spin information applications, systems with a single spin channel in a large gap would be ideal, as is the case of bare Bi_2Se_3. However, pristine surfaces are almost never of practical use. Oxidation of Bi_2Se_3 results in a complex band structure because of hybridization of the O-derived states with the substrate states. While the topological order is preserved, the spin current is much reduced. Thus, the often-cited robustness of the surface states in topological insulators does not imply conserved surface spin properties. Experiments performed on samples exposed to air or otherwise capped could be affected by interactions at the surface. Actual applications of topological materials will require a careful analysis of the effects of surface modification and interface formation in order to control or tailor the features and properties of interest.

This work was supported by the U.S. Department of Energy (Grant No. DE-FG02-07ER46383 for TCC) and the NUST Research Funding (No. 2011YBXM28, AB96377 for X. W.). X. W. acknowledges support by the China Scholarship Council (2009307164) and the Young Scholar Project of NUST (AB41382).

[1] L. Fu and C. L. Kane, Phys. Rev. B **76**, 045302 (2007).
[2] D. Hsieh, D. Qian, L. Wray, Y. Xia, Y. S. Hor, R. J. Cava, and M. Z. Hasan, Nature (London) **452**, 970 (2008).
[3] M. Z. Hasan and C. L. Kane, Rev. Mod. Phys. **82**, 3045 (2010).
[4] X. L. Qi and S.-C. Zhang, Rev. Mod. Phys. **83**, 1057 (2011).
[5] J. E. Avron, L. Sadun, J. Segert, and B. Simon, Phys. Rev. Lett. **61**, 1329 (1988).
[6] P. Roushan, J. Seo, C. V. Parker, Y. S. Hor, D. Hsieh, D. Qian, A. Richardella, M. Z. Hasan, R. J. Cava, and A. Yazdani, Nature (London) **460**, 1106 (2009).
[7] D. Hsieh *et al.*, Phys. Rev. Lett. **103**, 146401 (2009).
[8] T. Zhang *et al.*, Phys. Rev. Lett. **103**, 266803 (2009).
[9] H. Zhang, C. X. Liu, X. L. Qi, X. Dai, Z. Fang, and S. C. Zhang, Nature Phys. **5**, 438 (2009).
[10] Y. Xia *et al.*, Nature Phys. **5**, 398 (2009).
[11] Y. L. Chen *et al.*, Science **325**, 178 (2009).
[12] H. Lin, L. A. Wray, Y. Xia, S. Xu, S. Jia, R. J. Cava, A. Bansil, and M. Z. Hasan, Nature Mater. **9**, 546 (2010).
[13] X. Chen, X.-C. Ma, K. He, J.-F. Jia, and Q.-K. Xue, Adv. Mater. **23**, 1162 (2011).
[14] M. Bianchi, D. Guan, S. Bao, J. Mi, B. B. Iversen, P. D. C. King, and P. Hofmann, Nature Commun. **1**, 128 (2010).
[15] C. Chen *et al.*, arXiv:1107.5784.
[16] M. Bianchi, R. C. Hatch, J. Mi, B. B. Iversen, and P. Hofmann, Phys. Rev. Lett. **107**, 086802 (2011).
[17] D. Kong *et al.*, ACS Nano **5**, 4698 (2011).
[18] X. Gonze *et al.*, Z. Kristallogr. **220**, 558 (2005).
[19] X. Gonze *et al.*, Comput. Phys. Commun. **180**, 2582 (2009).
[20] See Supplemental Material at http://link.aps.org/supplemental/10.1103/PhysRevLett.108.096404 for additional data.
[21] Y. Zhang *et al.*, Nature Phys. **6**, 584 (2010).
[22] H. Chen, W. Zhu, D. Xiao, and Z. Zhang, Phys. Rev. Lett. **107**, 056804 (2011).
[23] J. A. Hutasoit and T. D. Stanescu, Phys. Rev. B **84**, 085103 (2011).
[24] K. P. Huber and G. Herzberg, *Molecular Spectra and Molecular Structure. IV. Constants of Diatomic Molecules* (Van Nostrand Reinhold, New York, 1979).
[25] H. Eschrig and M. Richter, Solid State Commun. **59**, 861 (1986).
[26] X.-L. Qi, and S.-C. Zhang, Phys. Rev. Lett. **101**, 086802 (2008).
[27] Y. A. Bychkov and E. I. Rashba, JETP Lett. **39**, 78 (1984).
[28] Y. A. Bychkov and E. I. Rashba, J. Phys. C **17**, 6039 (1984).